Study of a possibility to measure ESSνSB neutrino flux by observing elastic scatterings of neutrinos on orbital electrons

Kaja Krhač[1] and Budimir Kliček[2,*]

[1] *Department of Physics, University of Zagreb Faculty of Science*
[2] *Center of Excellence for Advanced Materials and Sensing Devices, Ruder Bošković Institute, HR-10000 Zagreb, Croatia*

(Dated: January 26, 2020)

Reconstruction of the muon (anti)neutrino flux in ESSnuSB may be feasible by observing elastic scattering of neutrinos on orbital electrons because the cross section for the process is known precisely. Total $\nu_\mu - e$ cross section was calculated using tree-level Feynman diagrams and is in excellent agreement with GENIE model. The main background to this process are $\nu_e(\overline{\nu}_e)$ charged current interactions with a nucleus. It was shown that the background can, in principle, be rejected by looking at energy and angle of outgoing electron with respect to the incoming neutrino. Further studies of detector response and event reconstruction are needed to determine whether this can be done in practice.

I. INTRODUCTION

ESSνSB (The European Spallation Source Neutrino Super Beam) [1] is a project whose goal is to measure CP violation in leptonic sector by comparing $\nu_\mu \to \nu_e$ and $\bar{\nu}_\mu \to \bar{\nu}_e$ oscillations.

To produce muon (anti)neutrino beam, protons are lead to collide with a target, producing hadrons which promptly decay to charged pions. A magnetic horn surrounding the target is used to select and focus positively or negatively charged pions. Then, pion beam enters the decay tunnel, thus yielding muon neutrino or muon antineutrino beam respectively by $\pi^\pm$ decay:

$$\begin{aligned} \pi^+ &\to \mu^+ + \nu_\mu \\ \pi^- &\to \mu^- + \bar{\nu}_\mu \ . \end{aligned} \tag{1}$$

In reality, the horns are not ideal, so the pion beam will predominantly consist of pions of the charge selected by the horn, with a contribution from pions of the opposite charge.

Furthermore, some of the muons (Eq. 1) will decay in the decay tunnel producing neutrinos of other flavours:

$$\begin{aligned} \mu^+ &\to \bar{\nu}_\mu + \nu_e + e^+ \\ \mu^- &\to \nu_\mu + \bar{\nu}_e + e^- \ . \end{aligned} \tag{2}$$

Other possible sources of contamination are secondary particles produced in hadron decay, like kaons, which are then also found in the pion beam.

In conclusion, the dominant component of neutrino beam is muon (anti)neutrino flux, but the beam will inevitably contain other neutrino flavour components.

Since the goal is to observe muon (anti)neutrino oscillations which are the source of CP violation signal, (anti)neutrino prompt flux component in the beam must be known precisely.

The flux is connected to the interaction rate $R(t)$ via cross section σ, by the equation

$$R(t) = \int_0^\infty \frac{dL(t)}{dE}\sigma(E)dE \ , \tag{3}$$

where $L(t)$ is the flux.

It can be seen from (3) that the flux can be determined if the interaction rate and the cross section are known.

In this work it is assumed that the interaction rate is measured using Cherenkov detector set at a distance of 250 m from the target. When neutrinos scatter either on nuclei or on orbital electrons, charged leptons and/or charged hadrons are produced, emitting Cherenkov radiation.

Neutrino-nucleus scattering cross section is not precisely known and is difficult to calculate because nuclear and chromodynamic effects must be taken into account [2]. On the other hand, neutrino-electron scattering cross section can be calculated in theory up to very high precision [3]. For this reason, the elastic scattering of neutrinos on orbital electrons is studied in order to measure neutrino flux.

The disadvantage is that the cross section for neutrino-electron scattering is about three orders of magnitude smaller than for neutrino-nucleus scattering because the cross section is proportional to the mass of the particle on which neutrino scatters. Since mass of an electron is approximately 2000 times smaller then mass of a nucleon, neutrino- electron cross section is at least three orders of magnitude smaller then neutrino-nucleus cross section. This means lower interaction rate.

Furthermore, the signal for this process is a single outgoing electron, which may also be a detected final state of electron (anti)neutrino charge-current (CC) interaction with a nucleus. It will be discussed how this background can be significantly reduced by looking at an angle of the outgoing electron.

In section II simulated interaction generator and analysis framework are described. section III discusses kinematics of elastic neutrino-electron scattering. Calcula-

* Mentor

tion of tree level cross section for elastic scattering of neutrino on electron and comparison with GENIE cross section model [4, 5] are given in section IV. In section V interaction rates are calculated and weighted properly. Finally, section VI covers the background processes and background reduction methods.

II. ANALYSIS

Neutrino interactions were simulated using GENIE Neutrino Monte Carlo Generator. GENIE[4, 5] stands for Generates Events for Neutrino Interaction Experiments and is a ROOT [6] based Neutrino Monte Carlo (MC) Generator. MC methods are a subset of computational algorithms that use the process of repeated random sampling to make numerical estimations of difficult to calculate quantities.

The set of physics models used in GENIE incorporates the dominant scattering models for wide range of energies where many different physical processes play out. The relativistic Fermi gas nuclear model is used for all processes and is most successful at lower end of energy range, while at high energies shadowing and similar effects are taken into account[4].

The analysis was done using ROOT Data Analysis Framework [6], a modular software toolkit commonly used in high energy physics that provides all the functionalities required to deal with data processing, visualisation etc.

III. KINEMATICS

The kinematics of elastic neutrino-electron scattering [7, 8] can be described by a single variable. It makes sense to choose θ_e, the angle between outgoing electron with respect to incoming neutrino because this variable can be measured. Energy of outgoing electron E_e can then be expressed as a function of energy of incoming neutrino E_ν and the angle θ_e.

It is assumed in the following derivation that the incoming neutrino has only z component of momentum, electron is initially at rest (Fig. 1), and scattered electron is ultra-relativistic (URL) so $E_e \gg m$, where m refers to the mass of electron:

$$\begin{aligned} p_1 &= (E_\nu, 0, 0, E_\nu) \\ p_2 &= (m, 0, 0, 0) \\ p_3 &= (E'_\nu, \vec{E}'_\nu) = (E_\nu + m - E_e, \vec{E}_\nu - \vec{E}_e) \\ p_4 &= (E_e, \vec{E}_e)\ . \end{aligned} \tag{4}$$

Conservation of energy and momentum was taken into account.

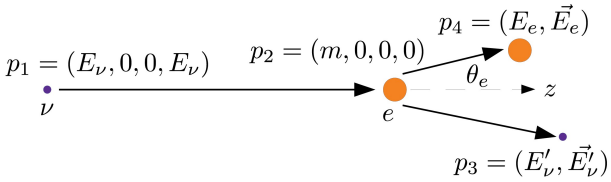

FIG. 1: Neutrino-electron scattering in laboratory system. Four-momentum of the incoming neutrino is p_1 and its four-momentum after the scattering is p_3. In the initial state, electron is at rest, so its four-momentum p_2 has only zeroth component which is equal to its mass, m. The four momentum of the final electron state is p_4.

To obtain expression for energy of outgoing electron E_e, one can look at conservation of invariant square of four-momentum:

$$(p_1 + p_2)^2 = (p_3 + p_4)^2\ . \tag{5}$$

Inserting (4) into above expression leads to:

$$mE_\nu = E_e(E_\nu + m - E_e) - E_\nu E_e \cos\theta_e + E_e^2\ . \tag{6}$$

It follows that:

$$E_e = \frac{mE_\nu}{E_\nu(1 - \cos\theta_e) + m}\ . \tag{7}$$

Defining variable $y = E_e/E_\nu$, which in the URL limit can be interpreted as the fractional energy loss of neutrino in the laboratory system:

$$y = \frac{E_\nu - E'_\nu}{E_\nu} = \frac{E_e - m}{E_\nu} \overset{\text{URL}}{\approx} \frac{E_e}{E_\nu}\ , \tag{8}$$

where in the second equality (4) was used, simplifies (7) to:

$$\begin{gathered} E_e(1 - \cos\theta_e) = m(1 - y) \\ \text{or} \\ 1 - \cos\theta_e = \frac{m}{E_e}(1 - y)\ . \end{gathered} \tag{9}$$

Since URL is assumed in derivation, the right-hand side is small. The angle on the left-hand side must then also be small meaning that electron is scattered in the forward direction. From here if follows that (9) is equal to:

$$E_e\theta_e^2 \approx 2m(1 - y)\ . \tag{10}$$

It can be shown that $E_e\theta_e^2$ is constrained. Range of y can be deduced from (7). When $\theta_e = 0$ then $y = 1$, while for $\theta_e = \pi$, $y = \frac{m}{2E_\nu + m} \approx 0$, because $E_\nu \gg m$ (in the energy range of interest, the worst case scenario is when pion decays from rest, $E_\nu \approx 30$ MeV).

Thus, $E_e\theta_e^2 \leqslant 2m$. Variable $E_e\theta_e^2$ will be an important parameter [7] in further analysis to discriminate between the signal and background, as is explained further in the text.

IV. CROSS SECTION FOR ELASTIC SCATTERING OF MUON NEUTRINOS ON ELECTRONS

A. Analytic calculation

Neutrino and electron are fundamental leptons so the cross section can be directly obtained using Feynman rules for electroweak interaction. The calculation of tree level cross section will be compared with GENIE [4, 5] cross section model that also includes next to leading order (NLO) corrections which contribute to the tree level diagram [3].

Kinematics are the following (see Fig. 1):

$$\begin{aligned} p_1 &= (E_\nu, 0, 0, E_\nu) \ , \\ p_2 &= (m, 0, 0, 0) \ , \\ p_3 &= (E'_\nu, \vec{E}'_\nu) \ , \\ p_4 &= (E_e, \vec{p}_e) = (E_\nu + m - E'_\nu, \vec{E}_\nu - \vec{E}'_\nu) \ . \end{aligned} \tag{11}$$

The only difference in kinematics with respect to (4) is that mass of the electron will not be neglected and as the independent variables E_ν and θ, the angle between incoming and outgoing neutrino, are chosen because the obtained expressions are in simpler form.

The differential cross section as a function of θ_e will also be given.

Cross section is calculated using the expression

$$\sigma = \frac{1}{(2\pi)^2} \frac{1}{4\sqrt{(p_1 p_2)^2 - m_1^2 m_2^2}} \int |M|^2 \delta^4(p_1 + p_2 - p_3 - p_4) \frac{d^3 p_3}{2E_3} \frac{d^3 p_4}{2E_4} \tag{12a}$$

$$= \frac{1}{(2\pi)^2} \frac{1}{4E_\nu m} \int |M|^2 \delta(E_\nu + m - E'_\nu - E_e(p'_\nu)) \frac{d^3 p'_\nu}{4E'_\nu E_e(p'_\nu)} \tag{12b}$$

$$= \frac{1}{(2\pi)^2} \frac{1}{4E_\nu m} \int |M|^2 \delta\left(f(p'_\nu)\right) \frac{p'^2_\nu dp'_\nu}{4p'_\nu E_e(p'_\nu)} d\Omega \tag{12c}$$

$$= \frac{1}{(2\pi)^2} \frac{1}{4E_\nu m} \int |M|^2 \left| \frac{df}{dp'_\nu} \right|^{-1}_{p'^*_\nu} \frac{p'^*_\nu}{4E_e(p'^*_\nu)} d\Omega \ . \tag{12d}$$

The delta function in (12a) makes sure that the four-momentum is conserved. To obtain (12b), (11) is substituted into (12a), then delta function is split into a part that takes care of conservation of energy and a part that takes care of conservation of three-momentum. Finally, it was integrated with respect to p_3.

Next, differential $d^3 p'_\nu$ is written in spherical form $p'^2_\nu dp'_\nu d\Omega$ and argument in the delta function in (12c) is defined as $f(p'_\nu)$:

$$\begin{aligned} f\left(p'_\nu\right) &= E_\nu + m - p'_\nu - E_e\left(p'_\nu\right) \\ &= E_\nu + m - p'_\nu - \sqrt{E_\nu^2 + p'^2_\nu - 2E_\nu p'_\nu \cos\theta + m^2} \ , \end{aligned} \tag{13}$$

where the conservation of three-momentum was used in the second line.

To evaluate the integral in (12c), the delta function must be written in the form $\delta(p'_\nu - p'^*_\nu)$, where p'^*_ν is the momentum of outgoing neutrino that satisfies conservation laws. By looking at (13), it can be seen that this can be formulated as $f\left(p'^*_\nu\right) = 0$.

Momentum of the outgoing neutrino is then equal to:

$$\begin{aligned} (E_\nu + m - p'^*_\nu)^2 &= E_\nu^2 + (p'^*_\nu)^2 - 2E_\nu p'^*_\nu \cos\theta + m^2 \\ p'^*_\nu &= E'^*_\nu = \frac{E_\nu m}{E_\nu(1 - \cos\theta) + m} \ . \end{aligned} \tag{14}$$

Following this, the derivative of f is calculated:

$$\frac{df}{p'_\nu} = -1 - \frac{p'_\nu - E_\nu \cos\theta}{E_e(p'_\nu)} \ . \tag{15}$$

Subsequently, by inserting (14) and (15) into (12d) the equation of the differential cross section is obtained:

$$\frac{d\sigma}{d\Omega} = \frac{1}{64\pi^2} \frac{1}{\left(E_\nu(1 - \cos\theta) + m\right)^2} |M|^2 \ . \tag{16}$$

Following the same procedure, but integrating with respect to p_4 instead of p_3, one arrives at the equation for the differential cross section as a function of the θ_e:

$$\frac{d\sigma}{d\Omega_e} = \frac{1}{64\pi^2} \frac{1}{E_\nu m} \frac{E_e^2 - m^2}{\left| E_e(\sqrt{E_e^2 - m^2} - E_\nu \cos\theta_e) + \sqrt{E_e^2 - m^2}(E_\nu + m - E_e) \right|} |M|^2 \ , \tag{17}$$

where E_e is energy of the outgoing electron and is equal to

$$E_e = m\frac{(E_\nu + m)^2 + E_\nu^2 \cos^2\theta_e}{(E_\nu + m)^2 - E_\nu^2 \cos^2\theta_e} \,. \tag{18}$$

To obtain the total cross section, (18) should be inserted into (17) which is much harder to integrate and that is why the total cross section will be calculated using (16).

The next step is calculating the square of the amplitude. In elastic muon neutrino-electron scattering, leptons exchange Z^0 boson. The Feynman diagram of the process is shown in Fig. 2.

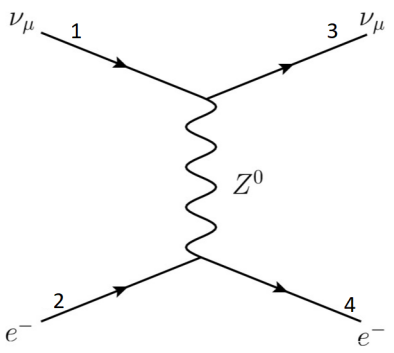

FIG. 2: Tree level Feynman diagram of elastic muon neutrino scattering on electron.

Using the Feynman rules for the weak interaction, the square of the amplitude is obtained as [9]

$$|M|^2 = 2G_F^2 \left[\bar{u}_3\gamma^\mu(c_V^{(1)} - c_A^{(1)}\gamma^5)u_1\right]\left[\bar{u}_4\gamma_\mu(c_V^{(2)} - c_A^{(2)}\gamma^5)u_2\right]\left[\bar{u}_1\gamma^\nu(c_V^{(1)} + c_A^{(1)}\gamma^5)u_3\right]\left[\bar{u}_2\gamma_\nu(c_V^{(1)} - c_A^{(1)}\gamma^5)u_1\right] \,, \tag{19}$$

where $G_F = \frac{1}{4\sqrt{2}}\frac{g^2}{m_W^2} = 1.166\,378\,7(6)\cdot 10^{-5}\ \mathrm{GeV}^{-2}$ [10] is Fermi constant. Constant θ_W is the Weinberg mixing angle and c_V and c_A are vector and axial coupling constants which depend on charge of the lepton. For muon neutrino $c_V^{(1)} = c_A^{(1)} = \frac{1}{2}$ and for electron $c_V^{(2)} = -\frac{1}{2} + 2\sin^2\theta_W$, $c_A^{(1)} = -\frac{1}{2}$, where $\sin^2\theta_W = 0.231\,22(4)$[10].

To calculate the cross section, all possible spin states must be taken into account. Since there are two possible initial state helicity configurations:

$$< |M|^2 >= \frac{1}{2}\sum_{\text{spins}} |M|^2 \,. \tag{20}$$

The next step is to write matrix multiplication in index form. With the use of completeness relation the result can be expressed in terms of traces:

$$\begin{aligned} < |M|^2 > = G_F^2 \Bigg\{ &\left[(c_V^{(1)})^2 + (c_A^{(1)})^2\right] \mathrm{Tr}(\not{p}_3\gamma^\mu\not{p}_1\gamma^\nu) + 2c_V^{(1)}c_A^{(1)}\mathrm{Tr}(\not{p}_3\gamma^\mu\not{p}_1\gamma^5\gamma^\nu)\Bigg\}\times \\ &\Bigg\{(c_V^{(2)})^2\,\mathrm{Tr}\Big(\gamma_\mu(\not{p}_2 + m)\gamma_\nu(\not{p}_4 + m)\Big) + c_V^{(2)}c_A^{(2)}\left[\mathrm{Tr}\Big(\gamma_\mu(\not{p}_2 + m)\gamma^5\gamma_\nu(\not{p}_4 + m)\Big) - \mathrm{Tr}\Big(\gamma_\mu\gamma^5(\not{p}_2 + m)\gamma_\nu(\not{p}_4 + m)\Big)\right] - \\ &(c_A^{(2)})^2\mathrm{Tr}\Big(\gamma_\mu\gamma^5(\not{p}_2 + m)\gamma^5\gamma_\nu(\not{p}_4 + m)\Big)\Bigg\} \,. \end{aligned} \tag{21}$$

Calculating traces and contracting the indices, previous expression simplifies to:

$$\begin{aligned} < |M|^2 > = 16G_F^2 \Bigg\{ &2\left[(c_V^{(1)})^2 + (c_A^{(1)})^2\right]\left[(c_V^{(2)})^2 + (c_A^{(2)})^2\right]\Big((p_1\cdot p_2)(p_3\cdot p_4) + (p_2\cdot p_3)(p_1\cdot p_4)\Big) + \\ &8c_V^{(1)}c_A^{(1)}c_V^{(2)}c_A^{(2)}\Big((p_1\cdot p_2)(p_3\cdot p_4) - (p_2\cdot p_3)(p_1\cdot p_4)\Big) - 2m^2\left[(c_V^{(1)})^2 + (c_A^{(1)})^2\right]\left[(c_V^{(2)})^2 - (c_A^{(2)})^2\right](p_1\cdot p_3)\Bigg\} \,. \end{aligned} \tag{22}$$

The last term in (22) is zero if the electron is URL. Scalar products of momenta are determined using (11).

After inserting the numbers for neutrino coupling constants and defining abbreviations:

$$\begin{aligned} g_+ &\equiv c_V^{(2)} + c_A^{(2)} \,, \\ g_- &\equiv c_V^{(2)} - c_A^{(2)} \,, \end{aligned} \tag{23}$$

the average of the amplitude squared is equal to

$$< |M|^2 >= 16 G_F^2 (E_\nu m)^2 \left\{ g_+^2 + g_-^2 \left(\frac{m}{E_\nu(1-\cos\theta)+m} \right)^2 - g_+ g_- \frac{m(1-\cos\theta)}{E_\nu(1-\cos\theta)+m} \right\} . \tag{24}$$

The final step consists of inserting (24) into (16) and integrating with respect to solid angle. Total cross section is equal to

$$\begin{aligned} \sigma &= \frac{G_F^2}{2\pi}(E_\nu m)^2 \int_0^\pi d\theta \sin\theta \frac{1}{(E_\nu(1-\cos\theta)+m)^2} \left\{ g_+^2 + g_-^2 \left(\frac{m}{E_\nu(1-\cos\theta)+m} \right)^2 - g_+ g_- \frac{m(1-\cos\theta)}{E_\nu(1-\cos\theta)+m} \right\} \\ &= \frac{G_F^2}{2\pi} E_\nu m \left[g_+^2 \left(1 - \frac{m}{2E_\nu + m} \right) + \frac{g_-^2}{3} \left(1 - \left(\frac{m}{2E_\nu + m} \right)^3 \right) - 2 g_+ g_- \frac{E_\nu m}{(2E_\nu + m)^2} \right] . \end{aligned} \tag{25}$$

Total cross section depends only on the energy of incoming neutrino and mass of electron, i.e. target.

The obtained cross section will be compared with the GENIE cross section model.

B. Comparison of tree level cross section with GENIE cross section model

The comparison of calculated tree level cross section (25) with GENIE model is shown in Fig. 3.

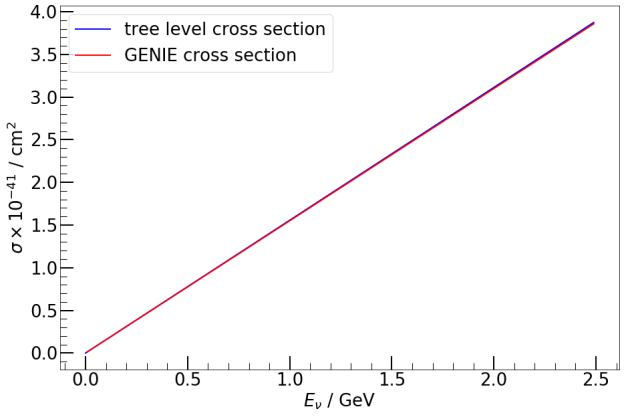

FIG. 3: Comparison of calculated cross section on tree level with GENIE cross section model.

Tree level cross section is in great agreement with GENIE cross section model which takes into account electroweak radiative corrections to tree level. They include full one loop electroweak corrections of the standard model and photon Bremsstrahlung effects [3], but one can conclude their contribution is insignificant up to approximatelly 2 GeV where it can be seen that lines start to deviate.

V. INTERACTION RATES

This section describes the formalism used to calculate the expected interaction rates of neutrino flux [11]. Interaction rate is defined as the number of neutrino interactions per unit time

$$R_{\text{int}}(t) \equiv \frac{dN_{\text{int}}(t)}{dt} \,, \tag{26}$$

where R_{int} is the interaction rate and N_{int} is a number of interactions as a function of time. It is connected to the flux via (3). The neutrino flux as a function of protons on target is defined as the number of neutrinos passing through a unit area in unit time

$$\tilde{L}(E) = \frac{d^3 N_\nu(t)}{dE\, dA\, dN_{\text{pot}}} \,, \tag{27}$$

where $N_\nu(t)$ is number of neutrinos passing perpendicularly through arbitrary flat surface of area A and N_{pot} is number of protons on target.

Number of protons on target, or just "protons on target (p. o. t.)", is the number of protons delivered to the neutrino generating target. In the following calculations, number of protons on target in a year (200 days or 5000 hours) is $2.16 \cdot 10^{23}$. The p. o. t. interaction rate is defined as

$$R_{\text{pot}} \equiv \frac{dN_{\text{int}}}{dN_{\text{pot}}} = \frac{dN_{\text{int}}}{\dot{N}_{\text{pot}}(t)dt} = \frac{R_{\text{int}}}{\dot{N}_{\text{pot}}(t)}\,, \tag{28}$$

One more adjustment of expression for interaction rate is needed. Note that the cross sections are defined for a single isotope of a single element, while detectors are defined by their chemical composition and macroscopic quantities. Thus, it is sensible to express interaction rate per p.o.t. per unit mass of target. If target is made of one element, then the total cross section is

$$\sigma_{\text{tot}} = N_N \cdot \sigma_E(E; Z, A)\,, \tag{29}$$

where N_N is a number of atoms present in the target and σ_E is the neutrino cross section of an element with atomic number Z and mass number A. Connection between mass of substance m and number of atoms is given through number of moles n:

$$n = \frac{m}{M} = \frac{N_N}{N_A}\,, \tag{30}$$

where M is molar mass and N_A is the Avogadro constant.

Finally, the number of expected interactions per p.o.t. in the target of mass m composed of a single element is

$$R^{\text{tot}}_{\text{pot}} = m\frac{N_A}{M}\int_0^\infty \tilde{L}(E)\sigma_E dE\,, \tag{31}$$

where $\tilde{L}(E)$ is defined in (27). Since scatterings of neutrinos in Cherenkov detector are studied, the target is water, and mass will be expressed in 10^6 kg (metric kilotonne). In the following, cross sections are given for a single molecule of water.

To calculate the expected number of interactions cross sections flux must be known.

A. Cross section

Total cross section and neutrino-electron cross sections obtained from GENIE are shown in Fig. 4.

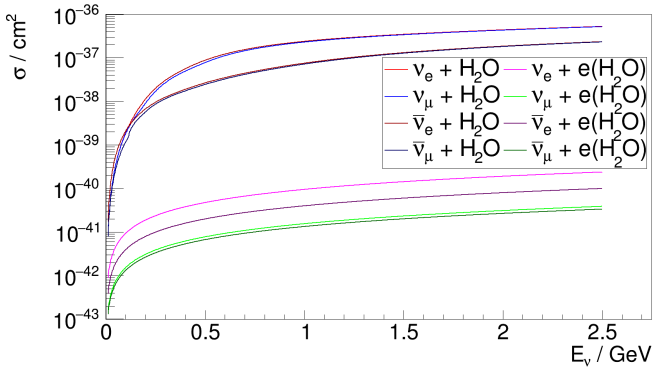

FIG. 4: Dependence of total cross section and neutrino-electron scattering cross section on neutrino energy for flavours of interest.

Total cross section includes scattering on both hydrogen and oxygen nucleus (two oxygen nuclei in fact, because there are two oxygen atoms in molecule of water) and their orbital electrons, while neutrino-electron cross section includes only scatterings on orbital electrons.

One of the reasons why the total cross section is a few orders of magnitude larger then neutrino-electron cross section is because cross section is proportional to mass of the particle on which neutrino scatters (Eq. 25).

B. Flux

Expected fluxes were obtained using FLUKA [12] simulation of neutrino production facility.

Prompt flux component of each neutrino flavour in neutrino beam for both positive and negative horn polarity is shown in Fig. 5. Positive horn polarity focuses and selects positively charged pions, while negative horn polarity focuses and selects negatively charged pions, thus producing dominantly muon neutrino or muon antineutrino beam, respectively.

Total flux in 200 days for all neutrino flavours for both positive and negative polarities are given in Tab. I and II, respectively.

TABLE I: Total flux of neutrinos in 200 days for positive horn polarity at 250 m from target.

neutrino	total flux / cm^2 / p.o.t. (200 days)	fraction / %
ν_μ	$6.9 \cdot 10^{13}$	$9.85 \cdot 10^{-1}$
ν_e	$3.4 \cdot 10^{11}$	$4.85 \cdot 10^{-3}$
$\bar{\nu}_\mu$	$6.9 \cdot 10^{11}$	$9.85 \cdot 10^{-3}$
$\bar{\nu}_e$	$4.3 \cdot 10^{9}$	$6.14 \cdot 10^{-5}$

There is a non-negligible electron neutrino and muon antineutrino flux component in the beam in case of positive polarity.

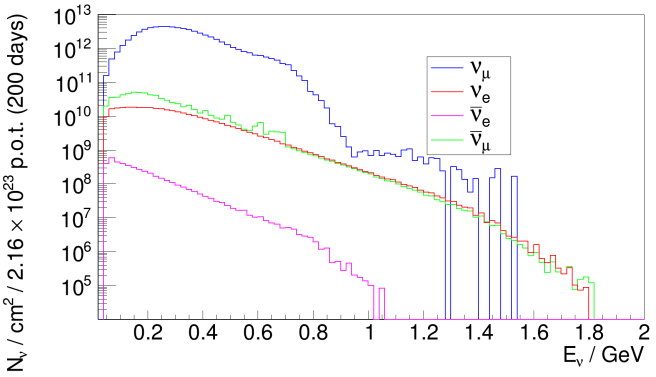

(a) Positive horn polarity

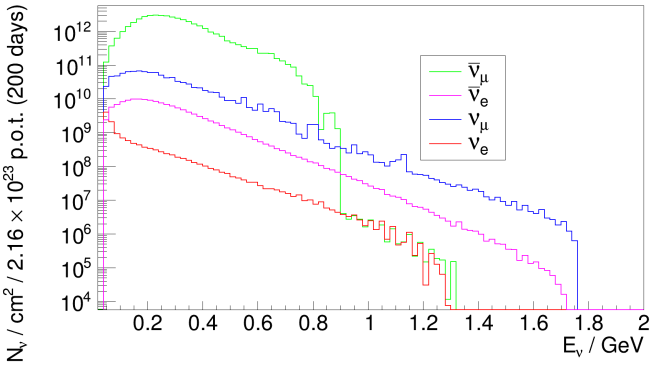

(b) Negative horn polarity

FIG. 5: Neutrino flux at 250 m from target for (a) positive horn polarity and (b) negative horn polarity with baseline current of 350 kA. Dominant flavour type for positive horn polarity are muon neutrinos, while dominant flavour type for negative horn polarity are muon antineutrinos.

TABLE II: Total flux of neutrinos in 200 days for negative horn polarity 250 m from target.

neutrino	total flux / cm^2 / p.o.t. (200 days)	fraction / %
ν_μ	$9.6 \cdot 10^{11}$	$2.23 \cdot 10^{-2}$
ν_e	$1.3 \cdot 10^{10}$	$3.02 \cdot 10^{-4}$
$\bar{\nu}_\mu$	$4.2 \cdot 10^{13}$	$9.74 \cdot 10^{-1}$
$\bar{\nu}_e$	$1.4 \cdot 10^{11}$	$3.25 \cdot 10^{-3}$

For negative horn polarity, non-negligible flux components are muon neutrinos and electron antineutrinos.

There are more muon neutrinos in positive horn polarity flux than muon antineutrinos in negative horn polarity flux, because protons and nuclei are positively charged. So, it is more probable that resulting mesons will be positively charged and positive pions decay into neutrinos.

C. Interaction rate

Neutrino interactions were simulated using GENIE Neutrino Monte Carlo Generator.

Number of simulated events does not necessarily represent the expected number of interactions. This is because the number of simulated interactions needs to be large enough to obtain enough statistics for the analysis. So, simulated interactions must be weighted properly before one can interpret the obtained simulation.

The weight of each simulated interaction is equal to the interaction rate of some scattering process, which is calculated using (31), divided by the number of such interactions in the MC simulation. In other words, weight is the ratio of expected number of interactions and simulated number of events, so that the integral of differential interaction rate is equal to the expected number of events.

Interaction rate in 1 kt of water in 200 days is shown in Fig. 6 for muon neutrinos in the case of positive horn polarity and muon antineutrinos in case of negative horn polarity.

Total interaction rates for all neutrino flavours in the flux are shown in Fig. 7.

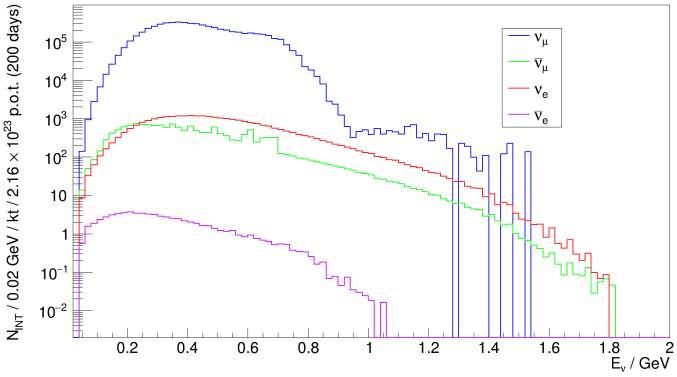

(a) Positive horn polarity

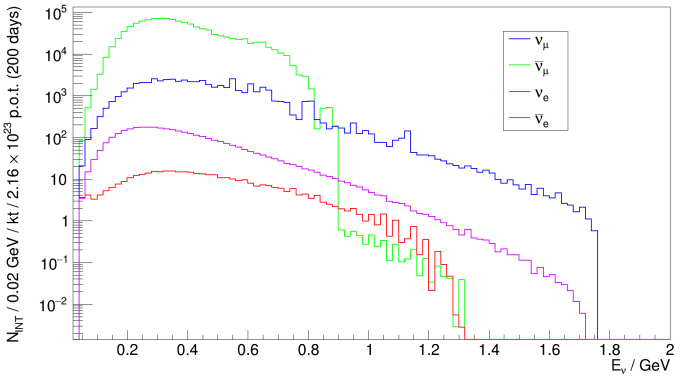

(b) Negative horn polarity

FIG. 7: Total interaction rate 250 m from target for (a) positive horn polarity and (b) negative horn polarity.

Expected number of interactions in 1 kt of water in

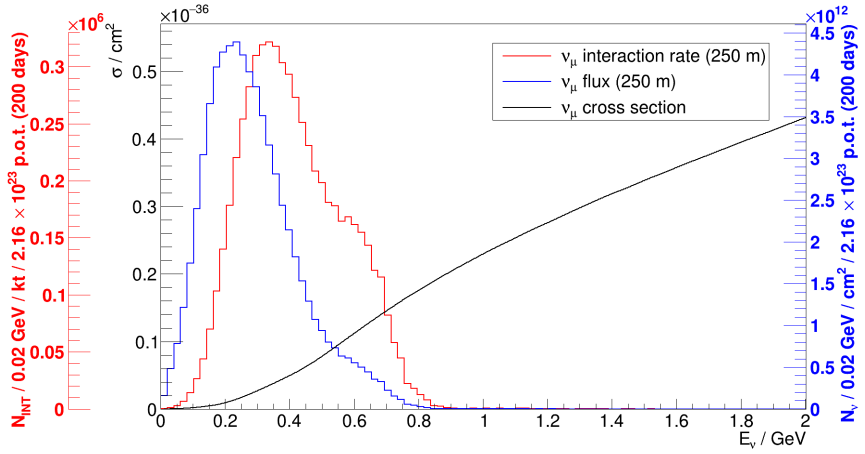

(a) Positive horn polarity - muon neutrinos

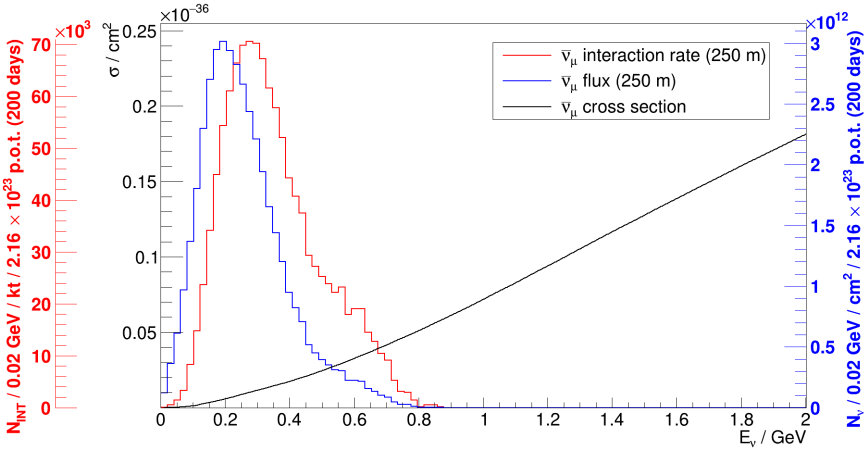

(b) Negative horn polarity - muon antineutrinos

FIG. 6: Cross section, flux and interaction rate 250 m from target for dominant flavour in two horn polarities. The red line is the interaction rate. Its peak is moved to the right with respect to the flux (blue line) because cross section (black line) is larger at larger energies.

200 days is given in Tab. III for positive horn polarity and IV for negative horn polarity.

TABLE III: Expected number of interactions in 1 kt of water in 200 days for positive horn polarity.

neutrino	expected number of interactions
ν_μ	6 017 320
ν_e	29 987
$\bar{\nu}_\mu$	15 896
$\bar{\nu}_e$	69

Even though the prompt flux component of muon antineutrinos (Tab. I) is almost two times larger than flux component of electron neutrinos in the beam, the cross section for scatterings of neutrinos is approximately three times larger than the one for antineutrinos [3]. When all is taken into account. it turns out that the interaction rate of electron neutrinos exceedes the one for muon antineutrinos.

TABLE IV: Expected number of interactions in 1 kt of water in 200 days for negative horn polarity.

neutrino	expected number of interactions
ν_μ	57 151
ν_e	390
$\bar{\nu}_\mu$	1 153 000
$\bar{\nu}_e$	3 410

The largest number of expected interactions, after the muon antineutrinos, are from muon neutrinos (Tab. II), which is expected because they are the second dominant flavour component in the flux and the cross section is larger than for antineutrinos.

Electron neutrino background will be discussed in the following section.

VI. BACKGROUND

The signal is elastic scattering of muon (anti)neutrinos on orbital electrons for the (negative) positive horn polarity. The signature of this process in the Cherenkov detector is a detected electron with no other detected particles.

The main source of background are CC interactions of electron (anti)neutrinos with nuclei, simply because neutrino-nucleus cross section is larger than neutrino-electron cross section, thus larger expected number of interactions. All other prompt flux flavour components also produce an electron (or positron) in the final state by scattering on orbital electrons, but this is a minor contribution to the background.

The processes where neutrino scatterings produce an outgoing electron or positron are given in Tab. V.

TABLE V: Process of neutrino scatterings that produce an outgoing electron. Nucleus is marked as N, while N' refers to all charged particles produced in CC interactions. Neutral current interaction is abbreviated as NC.

process	type of interaction
$\nu_\mu + e^- \to \nu_\mu + e^-$	NC
$\nu_e + e^- \to \nu_e + e^-$	CC-NC interference
$\nu_e + N \to N' + e^-$	CC
$\bar{\nu}_\mu + e^- \to \bar{\nu}_\mu + e^-$	NC
$\bar{\nu}_e + e^- \to \bar{\nu}_e + e^-$	CC-NC interference
$\bar{\nu}_e + N \to N' + e^+$	CC

There are other possibilities of neutrino and antineutrino scatterings but the energy threshold is higher than ESSνSB neutrino energies. For muon neutrino charged-current scattering:

$$\nu_\mu + e^- \to \mu^- + \nu_e \ , \tag{32}$$

the threshold for electron at rest is 10.8 GeV. To calculate energy threshold, one starts by calculating energy in the center of momentum (CoM) for the inital particles:

$$\begin{aligned} s &= (E_\nu + m_e)^2 - \vec{E_\nu}^{\,2} \\ &= 2E_\nu m + m_e^2 \ , \end{aligned} \tag{33}$$

where s is the Mandelstam variable. At the threshold, particles are created at rest, so energy must be at least equal to the sum of their masses:

$$2E_\nu m_e + m_e^2 = m_\mu^2 \ . \tag{34}$$

Expressing E_ν in the previous equations leads to:

$$E_\nu = \frac{m_\mu^2 - m_e^2}{2m_e} \ , \tag{35}$$

where neutrino mass has been neglected.

If muon neutrino is replaced with tau neutrino, the threshold is 3 TeV, which is unattainable, so they are not mentioned in the work.

A. Background reduction

The main background reduction technique is based on the fact that electrons produced in neutrino-nucleus scattering will scatter at a larger angle than electrons produced in neutrino-electron scatterings. This is because when mass of the target is larger than mass of the projectile, the projectile will scatter at a larger angle. In an extreme case where mass of the target is infinite, the projectile will scatter backwards and the target will remain at rest, like when a ball scatters off a wall.

The additional background reduction can be accomplished by noticing that when neutrino scatters off nucleus, charged particles (mostly charged pions) are produced and may also be detected in Cherenkov detector. Thus, if more than one charged particle is detected in the scattering, it is a clear sign that this is not the case of elastic neutrino-electron scattering. This kind of filtering will be referred to as Cherenkov filter in the text.

The distribution of angle of the outgoing electron is shown in Fig. 8.

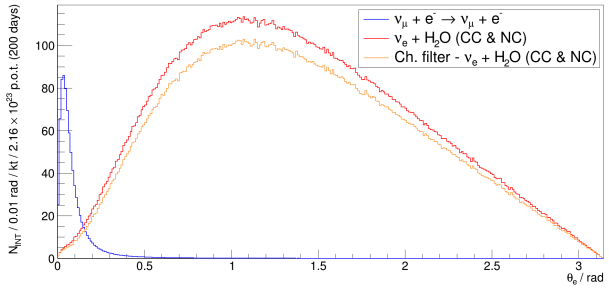

(a) Positive horn polarity

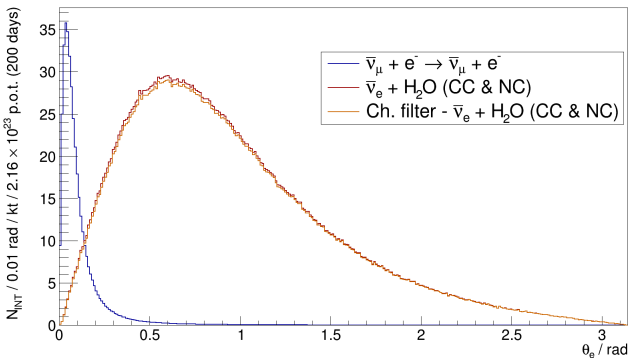

(b) Negative horn polarity

FIG. 8: Distribution of angle of the outgoing electron. The blue line represents the signal, while the dark red and yellow line represent electron neutrino scattering before and after applying the Cherenkov filter, respectively.

From Fig. 8, one can notice that peak of the muon signal is at small angles, while electron neutrino scattering signal peaks at larger angles meaning that the background comes mostly from electron neutrino-nucleus scattering. This is also where Cherenkov filter is the most effective.

Alternatively, one may look at the square of the angle of outgoing electron distribution. The distribution is shown in Fig. 9.

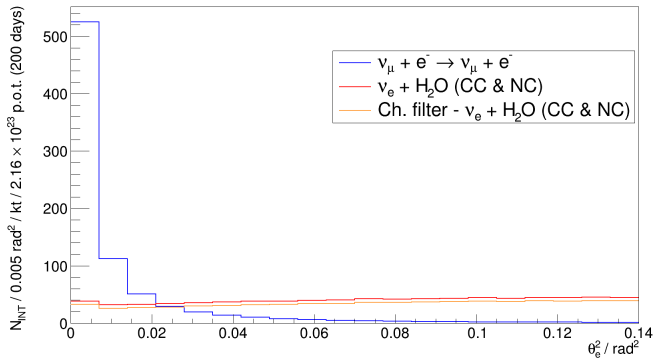

(a) Positive horn polarity

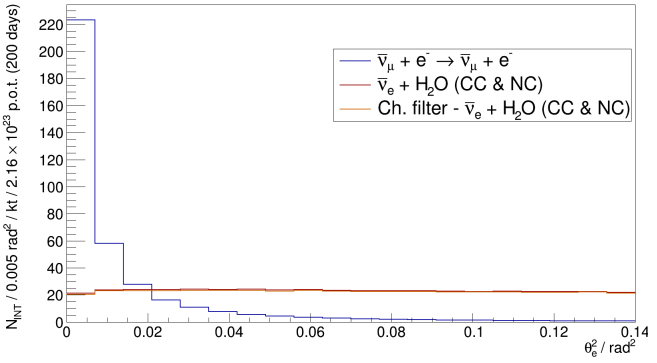

(b) Negative horn polarity

FIG. 9: Distribution of θ_e^2. The blue line represents the signal, while the dark red and yellow line represents electron neutrino scattering before and after applying the Cherenkov filter, respectively.

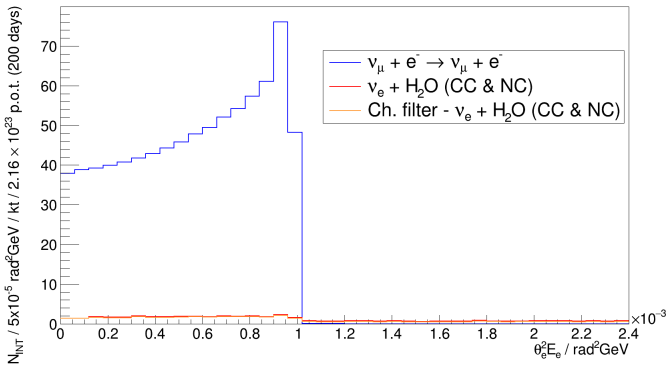

(a) Positive horn polarity

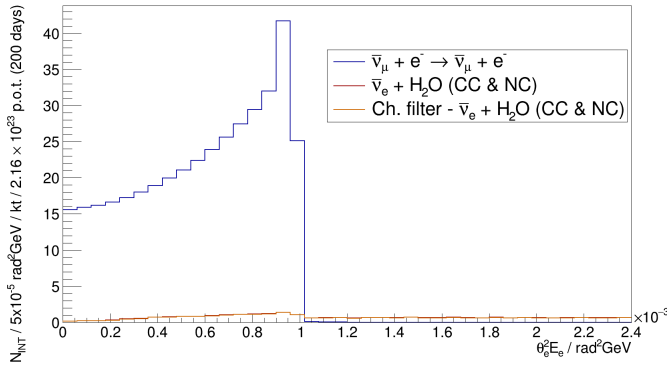

(b) Negative horn polarity

FIG. 10: Distribution of $\theta_e^2 E_e$. The blue line represents the signal, while the dark red and yellow line represent electron neutrino scattering before and after applying the Cherenkov filter, respectively. There is a sharp cut-off of the signal at $E_e\theta_e^2 = 2m_e$.

When looking at either θ_e or θ_e^2 distribution (Figs. 8 and 9), background at approximately 0.25 rad, or 0.02 rad^2, respectively, becomes larger than the signal. The goal is to try and find a parameter such that there is no signal lost in the background.

According to MINERvA [7], one should look at parameter $\theta_e^2 E_e$, where E_e is energy of the outgoing electron. In section III it was shown that $\theta_e^2 E_e$ variable is constrained, so that $\theta_e^2 E_e \leqslant 2m$. The distribution is shown in Fig. 10.

Background to signal ratio, in Fig. 10, is approximately 3.4 % for the negative horn polarity and 3.5 %. The stacked plot of the distribution of $\theta_e^2 E_e$, including the signal and all background processes is shown in Fig. 11.

In summary, predominant background for positive horn polarity comes from electron neutrino scatterings, while for negative horn polarity, it is electron antineutrinos (and muon neutrinos, see Fig. 11) that contribute the most. The CC electron (anti)neutrino-nucleus background may be reduced significantly by using $\theta_e^2 E_e$ as a discriminating parameter, which is constrained to the maximum value of $2m$. In this range the background to signal ratio is around 3.4%, and there is no signal overpowered by background. It can also be noticed that Cherenkov filter has little effect. Since this is the range of small outgoing electron angle values, the background comes from elastic electron neutrino-electron scattering where only electron is the outgoing particle. The mentioned discrimination methods are concerned only with CC electron (anti)neutrino-nucleus background. There is no way to discriminate between the signal and other aforementioned background processes of elastic scatterings of (anti)neutrinos on electrons (Tab. V).

VII. CONCLUSION

Muon-neutrino elastic scattering on electrons is a process whose cross section is known precisely. This possibly enables determination of (anti)neutrino prompt flux component in the beam. The main problem is the background from CC interactions of electron (anti)neutrinos with nuclei. It was shown that parameter $\theta_e^2 E_e$ has good background rejection potential, up to 3.4% compared to the signal in perfect conditions.

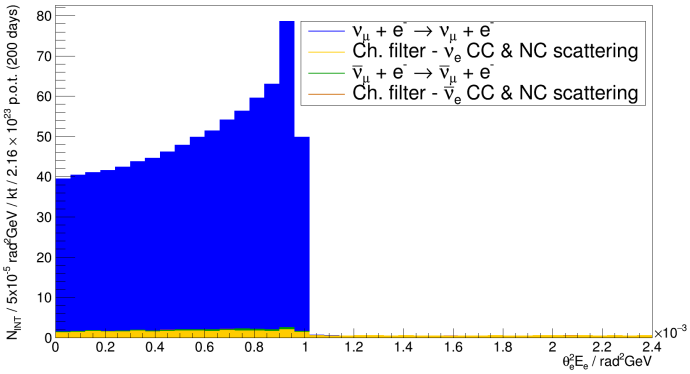

(a) Positive horn polarity

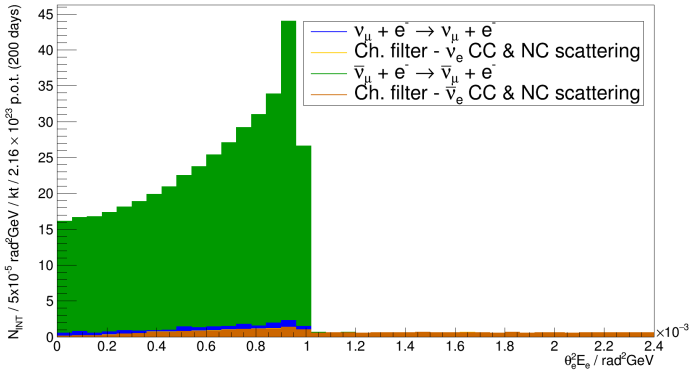

(b) Negative horn polarity

FIG. 11: Stacked plot of $\theta_e^2 E_e$ distribution. Dominant background in case of positive horn polarity comes from electron neutrinos (yellow), while in the case of negative polarity dominant backgorund is from electron antineutrinos (orange) and muon neutrinos (blue).

A possibly important background that was not studied is the coherent neutral current pion production. The two photons from π^0 decay could be detected as a single shower, mimicking the single electron signal. This requires further study.

This study demonstrated that the scattering of neutrinos on orbital electrons can, in principle, be observed using ESSνSB experimental setup. Further studies of detector response and event reconstruction are required to determine whether this can be done in practice.

[1] Marcos Dracos, Elian Bouquerel, Georgios Fanourakis, Gul Gokbulut, and Aysel Kayis Topaksu. The European Spallation Source Neutrino Super Beam Design Study. In *Proceedings, 10th International Particle Accelerator Conference (IPAC2019): Melbourne, Australia, May 19-24, 2019*, page MOPRB004, 2019.

[2] Anushree Ghosh. Charged Current Quasielastic Analysis from MINERA. In *Proceedings, 17th International Workshop on Neutrino Factories and Future Neutrino Facilities (NuFact15): Rio de Janeiro, Brazil, August 10-15, 2015*, pages 165–172, 2016.

[3] William J. Marciano and Zohreh Parsa. Neutrino electron scattering theory. *J. Phys.*, G29:2629–2645, 2003.

[4] C. Andreopoulos et al. The GENIE Neutrino Monte Carlo Generator. *Nucl. Instrum. Meth.*, A614:87–104, 2010.

[5] Costas Andreopoulos, Christopher Barry, Steve Dytman, Hugh Gallagher, Tomasz Golan, Robert Hatcher, Gabriel Perdue, and Julia Yarba. The GENIE Neutrino Monte Carlo Generator: Physics and User Manual. 2015.

[6] R. Brun and F. Rademakers. ROOT: An object oriented data analysis framework. *Nucl. Instrum. Meth.*, A389:81–86, 1997.

[7] E. Valencia et al. Constraint of the MINERνA medium energy neutrino flux using neutrino-electron elastic scattering. *Phys. Rev.*, D100(9):092001, 2019.

[8] S. Sarantakos, A. Sirlin, and W. J. Marciano. Radiative Corrections to Neutrino-Lepton Scattering in the SU(2)-L x U(1) Theory. *Nucl. Phys.*, B217:84–116, 1983.

[9] it is assumed that the momentum of exchanged boson q is negligible compared to mass of the exchanged boson m_Z, $q \ll m_Z$.

[10] P.J. Mohr, B.N. Taylor, and D.B. Newell. Codata recommended values of the fundamental physical constants: 1998. *Reviews of Modern Physics*, 80:633–730, 06 2008.

[11] Budimir Kliček. *Constraints on neutrino oscillation parameters implied by OPERA experiment data.* PhD thesis, University of Zagreb Faculty of Science, 2018.

[12] Alfredo Ferrari, Paola R. Sala, Alberto Fasso, and Johannes Ranft. FLUKA: A multi-particle transport code (Program version 2005). 2005.